A Review on Compliant Joints and Rigid-Body Constant Velocity Universal Joints Toward the Design of Compliant Homokinetic Couplings

Article *in* Journal of Mechanical Design · March 2015

DOI: 10.1115/1.4029318

CITATIONS
105

READS
11,429

3 authors, including:

Davood Farhadi
Delft University of Technology
19 PUBLICATIONS **215** CITATIONS

SEE PROFILE

Just L Herder
Delft University of Technology
329 PUBLICATIONS **5,103** CITATIONS

SEE PROFILE

A Review on Compliant Joints and Rigid-Body Constant Velocity Universal Joints Toward the Design of Compliant Homokinetic Couplings

D. Farhadi Machekposhti
Department of Precision and Microsystems Engineering,
Delft University of Technology,
Mekelweg 2,
Delft 2628 CD, The Netherlands
e-mail: d.farhadimachekposhti@tudelft.nl

N. Tolou[1]
Department of Precision and Microsystems Engineering,
Delft University of Technology,
Mekelweg 2,
Delft 2628 CD, The Netherlands
e-mail: n.tolou@tudelft.nl

J. L. Herder
Department of Precision and Microsystems Engineering,
Delft University of Technology,
Mekelweg 2,
Delft 2628 CD, The Netherlands
e-mail: j.l.herder@tudelft.nl

This paper presents for the first time a literature survey toward the design of compliant homokinetic couplings. The rigid-linkage-based constant velocity universal joints (CV joints) available from literature were studied, classified, their graph representations were presented, and their mechanical efficiencies compared. Similarly, literature is reviewed for different kinds of compliant joints suitable to replace instead of rigid-body joints in rigid-body CV joints. The compliant joints are compared based on analytical data. To provide a common basis for comparison, consistent flexure scales and material selection are used. It was found that existing compliant universal joints are nonconstant in velocity and designed based on rigid-body Hooke's universal joint. It was also discovered that no compliant equivalent exists for cylindrical, planar, spherical fork, and spherical parallelogram quadrilateral joints. We have demonstrated these compliant joints can be designed by combining existing compliant joints. The universal joints found in this survey are rigid-body non-CV joints, rigid-body CV joints, or compliant non-CV joints. A compliant homokinetic coupling is expected to combine the advantages of compliant mechanisms and constant velocity couplings for many applications where maintenance or cleanliness is important, for instance in medical devices and precision instruments.
[DOI: 10.1115/1.4029318]

Keywords: compliant mechanisms, spatial mechanisms, flexure, CV joints, homokinetic coupling

1 Introduction

Many applications require transmission of rotation from one direction to another with constant velocity, such as power transmission systems, parallel robot manipulators [1], rehabilitation and medical devices [2,3]. The primitive and traditional method to solve the problem of rotational transmission was Hooke's universal joint. A Hooke's universal joint includes three similar sets of four-bar spherical linkages that move in synchrony. However, Hooke's universal joint has a nonconstant velocity transfer function. As the angle between the two shafts increases, the variation in speed increases correspondingly. This causes increased stresses on universal joint members and a destructive vibration on the driven shaft [4]. Hunt proposed a general theory for constructing CV joints to overcome this problem [5]. Additionally, different types of CV joints, known as homokinetic coupling, have been presented that include Double Hooke, Rzeppa [6], Culver [7], Thompson [8], and Kocabas [9].

All of the CV and non-CV joints mentioned above are rigid-body mechanisms. Rigid-body configurations have many disadvantages, such as wear, friction, backlash, the need for maintenance and are generally cost ineffective. Besides, they sometimes work inside a vacuum, wet or dirty environment. Therefore, it is difficult to use conventional bearings, due to the need for lubrication [10]. Moreover, the backlash in rigid-body mechanical connections also can become a problem in high precision applications. To overcome these problems, compliant mechanisms can be used.

Compliant mechanisms transfer motion, force, or energy by using the elastic deformation of its flexure joints rather than using rigid-body joints only. Traditional joints offer near zero stiffness around a given set of axis or a surface and large stiffness along the other directions. However, this feature is difficult to achieve in compliant joints due to the internal stiffness that comes along with the compliancy of the structure. Therefore, the input energy is not transferred completely to the output part of the mechanism, and instead is stored in the elastic members. However, it has been shown that the deformation energy is not dissipated; it is stored and thereby conserved [11]. An advantage of compliant mechanisms is that they can easily be fabricated as a monolithic structure due to its hinge-less nature in design. This reduces wear, friction, and backlash in the mechanism and correspondingly increases precision, vital in the design of high-precision instrumentation [10]. However, compliant homokinetic coupling were not found in literature and clearly their design is not trivial.

This work aims to cover the knowledge-gap between compliant mechanisms and CV joints by performing a review toward the design of compliant homokinetic couplings. To this end, the following subobjectives are defined: (1) introducing feasible approaches to design compliant homokinetic couplings. (2) Presenting a literature survey on rigid-body CV joints, classification, and their graph representation. (3) Presenting an overview of different kinds of equivalent compliant configurations of used rigid-body joints in rigid-body CV joints, and comparing their performance based on analytical data such as range of motion,

[1]Corresponding author.

Contributed by the Mechanisms and Robotics Committee of ASME for publication in the Journal of Mechanical Design. Manuscript received December 28, 2013; final manuscript received December 3, 2014; published online January 15, 2015. Assoc. Editor: Chintien Huang.

axis drift, and stiffness in different directions. (4) Achieving equivalent compliant joints of used rigid-body joints in rigid-body CV joints which are nonexistent in compliant form.

The paper is structured as follows. In Sec. 2, the search method and design methods for compliant spatial mechanism are explained, including rigid-body-replacement method and the freedom and constraints topologies (FACT) method. Moreover, the methods for classification of the results, criteria selection, and evaluation of rigid-body CV joints and compliant joints are presented in this section. Section 3.1 presents the results of the literature review on rigid-body CV joints. Section 3.2 presents the available analytical results and their comparisons for compliant joints which are suitable to design compliant homokinetic couplings, including the compliant revolute joints, compliant universal joints, compliant spherical joints, and compliant translational joints. Section 4 discusses the results of each objective. Finally conclusions are presented in Sec. 5.

2 Methods

2.1 Design Methodologies. Two methods have been found to design compliant spatial mechanisms: the rigid-body-replacement method and the FACT.

2.1.1 Rigid-Body-Replacement Method. Rigid-body-replacement method consists of finding rigid-body mechanisms that accomplish the desired function. Based on the rigid-body mechanisms, a pseudo-rigid-body model is created that is converted into a compliant mechanism [12,13]. This was achieved by replacing the rigid-body joints with torsion springs representing compliant joints [10]. Therefore, to design a compliant homokinetic coupling using the rigid-body-replacement method, the rigid-body CV joints and suitable compliant joints to replace instead of rigid-body joints, should be investigated.

2.1.2 FACT Method. The FACT method is based on translating a mechanism's motion into degrees of freedom (DOF) that is used to find the geometric entities that describe the motion in the freedom space [14,15]. Knowing these geometric entities, it is possible to find the topology of a mechanism to generate the desired motion within the constraint space. Therefore, to design a compliant homokinetic coupling via this method, the geometric requirements for producing constant velocity transfer function and two rotational DOF between input and output shafts of coupling should be found.

2.1.3 Comparison of Rigid-Body-Replacement Method and FACT Method. Both rigid-body-replacement and FACT methods are able to design a three-dimensional and multiaxis flexure system such as homokinetic coupling. In comparison with FACT method, the rigid-body-replacement method is easier to apply if there is a desired rigid-body mechanism, and also if the compliant form of used rigid-body joints in the rigid-body mechanism is existing. This method is also a powerful method to model a compliant mechanism as a rigid-body linkage that emulates the behavior of the compliant mechanism under study. However, the FACT method is a synthesis method and can present all possible designs that would satisfy a specific motion requirement such as rotation transmission. Moreover, based on the FACT method, designer can be assured that all design concepts are considered [12–15].

2.2 Search Method. In order to perform the literature survey, both CV joints and as a secondary level, compliant joints were searched. The literature search was organized by using three search engines that the mechanism articles are indexed on them, including Scopus, Espacenet, and Google Patent Search. Scopus was used for journal articles and conference proceeding, while Espacenet and Google Patent Search were used to search for patents. To ensure finding the most related article, search terms were classified and combined. In total four different sets of keywords have been used, concerning keywords defining: (1) universal joints, (2) constant velocity, (3) compliant mechanisms, and (4) flexure joints.

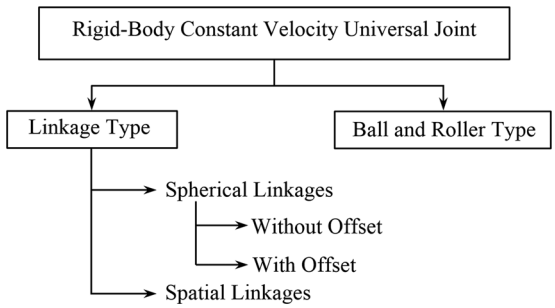

Fig. 1 Schematic representation of the classification levels to compare the rigid-body CV joints

2.3 Classification. In Fig. 1 a schematic representation of the classification to compare the rigid-body CV joints is shown. The first level describes the contact type between members of rigid-body CV joints, which are ball and roller type, and linkage type. The ball and roller type is characterized by point and line contact between the balls and rollers with their grooves in the yokes of the shafts, respectively, whereas the linkage type is characterized by surface contact between the links [16].

In the following, we limit ourselves to the linkage type because the ball and roller type has five shortcomings which are: (1) low misalignment angle, (2) low power transmission, (3) difficult to be converted into compliant embodiment, (4) low axial load capacity, and (5) locking and high wear under high loads. In the second level, a distinction was made between the spherical and spatial geometry of the linkage type rigid-body CV joints. In a spherical linkage any point in a moving frame is limited to move within a spherical surface, and all spherical surfaces of motion are concentric [4]. Besides, the spherical rigid-body CV joints have two types, with and without offset [17]. In spatial linkages at least there is a link in the system that moves between two general positions in space. Six parameters for specification of the location of this link are needed, three translational movements of a reference point and three rotations of the body about this point [18].

Compliant joints, flexure joints, or flexible joints, allow different kinematic DOF between connected parts with a monolithic structure. Some examples of compliant joints are revolute, translational, universal, spherical, and parallelogram quadrilateral joints. In the last 50 years, many compliant joints have been studied and developed, most of which fall into two categories: primitive flexures and complex flexures, combinations of two or more simple flexures [19]. The primitive flexure joints can be categorized as small-length flexural pivots and long flexible segments [20]. The small-length flexure pivots include notch type joints while long flexible segments include the curve-beam, leaf spring, tape spring, and contact-based.

2.4 Criteria Selection and Evaluation. Two most important criteria to compare the rigid-body CV joints are:

— *Misalignment Angle* is the angle between the input and output shafts.
— *Constant Velocity Condition* the ratio of output velocity to input velocity is to be constant at all angle of rotation. This criterion can be separated into two categories: near constant velocity and true constant velocity.

A preferred rigid-body CV joint has true constant velocity with high misalignment angle. Three most important criteria to compare the compliant joints are [21]:

— *Range of Motion* defined as the motion between the deflection limits to keep away from material failure. When the stress exceeds the yield stress, elastic deformation becomes plastic, after which joint behavior is unstable and uncertain which is not acceptable in precision engineering.
— *Axis Drift* defined as deviation of the center of rotation in compliant revolute joints and straight-line motion of compliant translational joints from their origin axes. Low axis drift is critical to achieve a precise kinematics.
— *The Ratio of Off-Axis Stiffness to On-Axis Stiffness* defined as the ratio of the stiffness in the undesired directions to the desired direction. In most applications a high ratio of off-axis stiffness to on-axis stiffness is desired.

For comparison of compliant joints with above mentioned criteria, all of the compliant joints were modeled analytically and the all flexible segments are considered in realm of linear beam theory. Moreover, to provide a common basis for comparison, consistent flexure scales and material selection were used.

3 Results

3.1 Rigid-Body CV Joints. Several different types of rigid-linkage-based CV joints exist. The one-to-one angular velocity ratio between the input and output shaft is associated with a symmetry of the CV joint about a plane called the homokinetic plane, which bisects the two shaft axes perpendicularly [5,22]. Therefore, the graph representation for a rigid-body CV joint is symmetric. Therefore, a symmetrical design as a geometric requirement is required for designing a compliant homokinetic coupling. An overview of results for the linkage type rigid-body CV joints, including graph representation, constant velocity condition, size, misalignment angle, the types of used rigid-body joints, and important combinations are shown in Table 1. In this table for most cases the graph representation was achieved and shown in Fig. 2. Revolute (R), prismatic (P), cylindrical (C), spherical (S), and planar (E) are different types of used rigid-body joints and spherical fork joint (F), Hooke's universal joint (H), and spherical parallelogram quadrilateral joint (Q) are important combinations.

3.2 Compliant Joints for Compliant Homokinetic Coupling. In Sec. 3.1, the types of used rigid-body joints and important combinations in rigid-body CV joints have been identified. The compliant form of the used rigid-body joints are compliant revolute joint, compliant universal joint, compliant spherical joint, and compliant translational joint. In this section, these compliant joints are classified and their stiffness, axis drift, and range of motion are investigated by using analytical model. There are no equivalent compliant joints for the planar, cylindrical, spherical fork, and spherical parallelogram quadrilateral joints. However, planar fork joint and planar parallelogram quadrilateral joints exist.

For comparison a high strength aluminum wrought alloy $Alcu_4Mg_1$ (EN AW 2024) is selected throughout this work. The relevant material specifications are $E = 70\,\text{GPa}$, $\nu = 0.33$, and $S_y = 440\,\text{MPa}$.

3.2.1 Compliant Revolute Joints. The compliant revolute joints are designed to create pure rotational motion. However, they have achieved a near rotational motion. Several different types of compliant revolute joints exist as shown in Fig. 3. In these figures, t, b, and L are thickness, width, and length of flexible segments, respectively. Parabolic, hyperbolic, elliptical, and cycloidal flexure hinges have same configuration as Fig. 3(*d*). In compliant revolute joints of Figs. 3(*f*)–3(*j*), φ denotes half of the angle between two leaf springs. Besides, in Fig. 3(*k*), φ_1 and φ_2 denote half of the angle between two inner leaf springs and two outer leaf springs, respectively. For the multileaf flexure joint, Fig. 3(*o*), all the leaf springs are same in length. Overviews of all the available analytical results, including range of motion, axis drift, on-axis stiffness, and off-axis stiffness, and flexure type are shown in Table 2. The geometric parameters values used for comparison are listed in Table 3. The related formulas for the given results in Table 2 are presented in the Supplementary Material (Appendix A) [65].

3.2.2 Compliant Universal Joints. A compliant universal joint allows two rotational DOF. Several compliant universal joints exist as shown in Fig. 4. All of them are based on rigid-body Hooke's universal joint and created by rigid-body-replacement

Table 1 Overview of the results of the linkage type rigid-body CV joints, including graph representation, size, misalignment angle, the types of used rigid-body joints, and important combinations. Graph representation shown in Fig. 2. Dash (—) denotes the results are not available; combinations not found identified with Ø.

				Criterion				
		Reference	Graph representation	Constant velocity condition	Size	Misalignment angle (deg)	The types of used rigid-body joints	Important combinations
Spherical linkage	Without offset	Rineer [23]	Fig. 2(*a*)	True	Small	Under 20	R, P	F
		Thompson [8]	Fig. 2(*b*)	True	Medium	30	R	Q,H
		Kocabas [9]	Fig. 2(*c*)	True	Medium	45	R	Q
	With offset	Double-Hooke [24]	Fig. 2(*d*)	Near	Large	20	R	H
		Geisthoff-1 [25]	Fig. 2(*e*)	Near	Large	40	R, S	H
		Geisthoff-2 [26]	Fig. 2(*f*)	True	Large	80	R, S	H
		Wier [27]	Fig. 2(*g*)	Near	Medium	90	R	Ø
Spatial linkage		Fenaille [28,29]	Fig. 2(*h*)	True	Medium	20	R, E	Ø
		Clemens [30]	Fig. 2(*i*)	True	Medium	Under 20	R, S	Ø
		Altmann [30]	Fig. 2(*j*)	True	Medium	Under 20	R, P, S	Ø
		Myard [30]	Fig. 2(*k*)	True	Medium	Under 20	R, C	Ø
		Dodge [31]	—	True	Medium	—	—	Ø
		Myard, et al [30]	Fig. 2(*l*)	True	Medium	Under 20	R	Ø
		Derby [30]	Fig. 2(*m*)	True	Large	Under 20	R, P	Ø
		Baker [32]	Fig. 2(*n*)	True	Medium	Under 20	R, C, S	Ø
		Culver [7]	Fig. 2(*o*)	True	Medium	90	R	Ø
		Eccher [33]	—	True	Large	45	—	Ø
		J. Falk [34]	—	True	Large	45	—	Ø
		Yaghoubi [35]	Fig. 2(*p*)	True	Medium	135	R, C	Ø

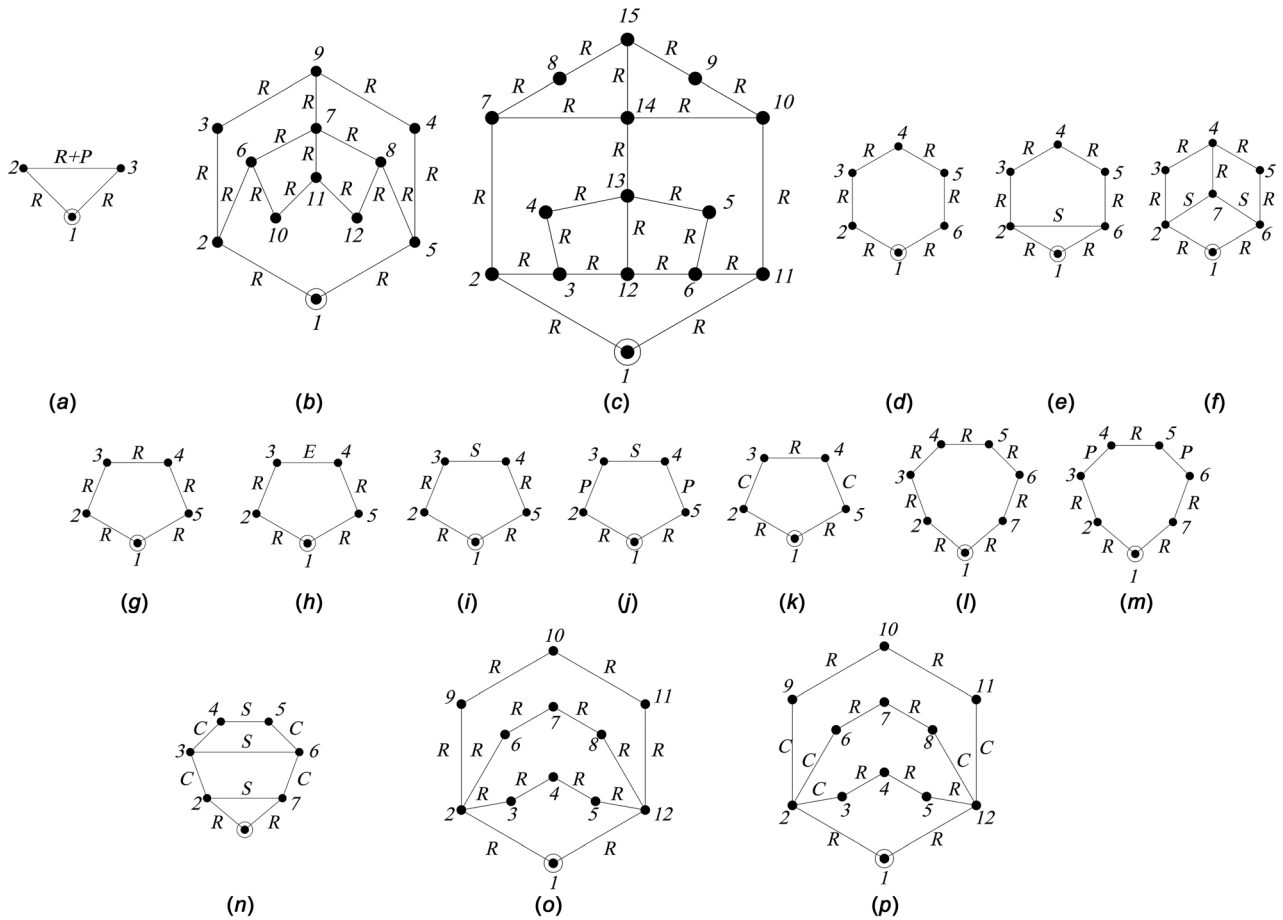

Fig. 2 Graph representation for linkage type rigid-body CV joints

method. According to Eq. (1), these joints transmit rotation with a nonlinear transfer function

$$\omega_{\text{out}} = \omega_{\text{in}} \times \cos\beta \tag{1}$$

where β is misalignment angle. Overviews of all the available analytical results, including range of motion, axis drift, on-axis stiffness, and off-axis stiffness, and flexure type are shown in Table 4. The compliant universal joints depicted in Figs. 4(*b*)–4(*d*), 4(*g*), and 4(*i*) are complex joints and include some circular and rectangular notch joints, respectively. Also the CU Joint and the X_{U}-joint, Figs. 4(*e*) and 4(*f*), include two CR-1 joints and two X_{R}-joints, respectively. Therefore, the results for the range of motion and axis drift in two on-axis directions, *z*-axis and *y*-axis, can be provided directly from the results of Table 2. Moreover, the related formulas for the other given results in Table 4 are provided in the Supplementary Material (Appendix B) [65].

3.2.3 Compliant Spherical Joints. A compliant spherical joint allows three rotational DOF, as does its traditional mechanical counterpart. Two compliant spherical joints exist as shown in Fig. 5. Overviews of all the available analytical results, including range of motion, axis drift, on-axis stiffness, and off-axis stiffness are shown in Table 5. The complex flexure joint shown in Fig. 5(*b*) is built by connecting CU Joint and CR-3 joint. Therefore, the results for the range of motion and axis drift in three on-axis directions, *z*-axis, *y*-axis, and *x*-axis can be provided directly from the results of Table 2. Moreover, the other related formulas for the given results in Table 5 are presented in the Supplementary Material (Appendix C) [65]. The geometric parameter values used for three-axis flexure joint are $L = 8$ mm, $t = 2$ mm, and $R = 4$ mm.

3.2.4 Compliant Translational Joints. Several compliant translational joints exist as shown in Fig. 6, which are complex flexures. A compliant translational joint allows one translational degree of freedom along *u*-axis. The compliant translational joints which depicted in Figs. 6(*a*)–6(*c*), and Figs. 6(*d*)–6(*i*) are including some circular notch joints and leaf springs, respectively. In this study, the compliant translational joints with planar configuration are investigated. However, several spatial compliant translational joints for reduced axis drift are presented in Refs. [21,70] and [71]. For comparison, the range of motion of the compliant translational joints is defined as a dimensionless parameter [72]

$$\delta^* = \frac{\delta_x}{\sqrt{G^2 + D^2}} \tag{2}$$

where G and D are width and length of compliant translational joint, respectively, and δ_x is the range of motion. Overviews of all the available analytical results, including range of motion, on-axis stiffness, and off-axis stiffness are shown in Table 6. The related formulas for the given results in Table 6 are provided in Supplementary Material (Appendix D) [65].

4 Discussion

4.1 Rigid-Body CV Joints. As can be seen in Table 1, Geisthoff-2, Culver, and Yaghoubi are true CV joints and have high allowable misalignment angle, i.e., more than 70 deg. As shown in the graph representation, Fig. 2, Double-Hooke, Geisthoff-1, Geisthoff-2, and Thompson have graphs with one, three, four, and six circuits, respectively, and they have the same outer circuits which represent two Hooke's universal joint in

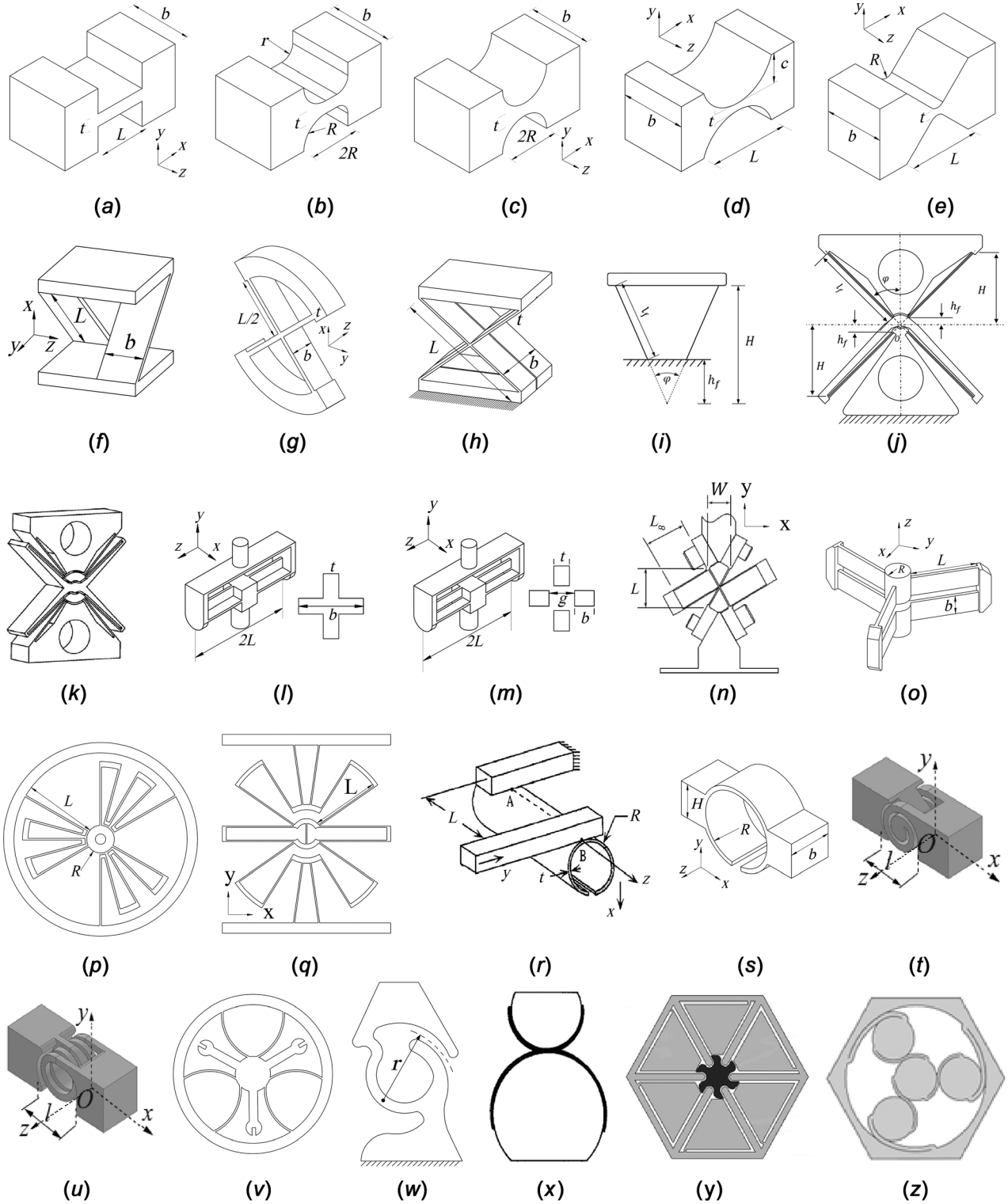

Fig. 3 Compliant revolute joints; (*a*) rectangular, (*b*) RCCF, (*c*) circular, (*d*) "a" parabolic, "b" hyperbolic, "c" elliptical, "d" cycloidal, (*e*) V-shape, (*f*) cross axis, (*g*) cartwheel, (*h*) X2, (*i*) LITF, (*j*) ADLIF, (*k*) butterfly, (*l*) CR-1, (*m*) CR-2, (*n*) ∞-flexure hinge, (*o*) CR-3, (*p*) multileaf, (*q*) multileaf spring, (*r*) split-tube-1(ST-1), (*s*) ST-2, (*t*) spiral, (*u*) helical, (*v*) annulus-shape, (*w*) revolute pair, (*x*) XR-joint, (*y*) contact-aided, and (*z*) rolling contact-2

series combination. Considering Thompson and Kocabas graph representations, two 4R circuits are alongside each other and show a spherical parallelogram quadrilateral joint which is also an important combination in these CV joints. As can be seen in the graph representation, Culver and Yaghoubi have same configuration and their difference is in selection of joints and geometric parameter values. Moreover, the graph representations of these two universal joints are combination of three similar circuits. Each circuit is based on Double Hooke's universal joint configuration with different types of rigid-body joints. According to the graph representation of Yaghoubi's universal joint, and the definition of a homokinetic coupling, the number of joints should be

Table 2 Overview of the compliant revolute joints, with flexure type (indicated with •), range of motion, axis drift, on-axis and off-axis stiffness; Dash (—) denotes the analytical data are not available. The embodiment of each joints showed in Fig. 3.

	Flexure type									On-axis stiffness	Off-axis STIFFNESS				
										$K_{\theta z}$	$K_{\theta y}$	$K_{\theta x}$	K_z	K_y	K_x
Compliant revolute joints	Primitive flexure	Complex flexure	Notch-type	Leaf-spring	Tape-spring	Curve-beam	Contact-base	Range of motion θ_z (rad)	Axis drift δ_z (μm)	N·mm/rad × 10^{-3}			N/mm × 10^{-3}		
Fig. 3(*a*) [36–39]	•		•					0.113	198.7	6.481	648.15	246.1	24	0.24	77.78
Fig. 3(*b*) [40]	•		•					0.06	4.2	0.112	—	—	—	—	—
Fig. 3(*c*) [36–39]	•		•					0.03	34	23.342	1267.6	485.33	55.05	1.153	152.11
Fig. 3(*d*)-a [41,42]	•		•					—	—	20.43	—	—	—	15.53	265.04
Fig. 3(*d*)-b [41,42]	•		•					—	—	7.103	—	—	—	77.4	164.64
Fig. 3(*d*)-c [42,43]	•		•					—	—	23.342	1267.6	—	—	57.186	152.11
Fig. 3(*d*)-d [44]	•		•					—	—	36.12	1832	—	80.66	1.758	109.84
Fig. 3(*e*) [44]	•		•					—	—	34.142	1585.1	—	68.15	1.642	94.99
Fig. 3(*f*) [38,45,46]		•		•				1.676	6620	0.0079	5.6	2.11	0.042	0.00006	4.2
Fig. 3(*g*) [38]		•		•				0.419	82.8	0.0315	22.4	8.433	0.672	0.0009	16.8
Fig. 3(*h*) [47]		•		•				0.838	130	0.0078	1.4	0.529	0.042	0.0002	4.2
Fig. 3(*i*) [48,49]		•		•				0.173	34	0.094	11.2	4.22	0.336	0.00047	8.4
Fig. 3(*j*) [48–51]		•		•				0.346	11.9	0.047	5.6	2.1	0.168	0.00024	4.2
Fig. 3(*k*) [48–52]		•		•				0.35	—	0.021	2.8	1.054	0.084	0.00012	2.1
Fig. 3(*l*) [21]		•		•				0.558	0	0.0941	358.52	358.52	33.29	10.76	10.76
Fig. 3(*m*) [21]		•		•				0.267	0	0.126	89.73	89.73	33.6	2.7	2.7
Fig. 3(*n*) [53]		•		•				—	—	—	—	—	—	—	—
Fig. 3(*o*) [21]		•		•				1.4	—	0.0057	—	—	1.01	—	—
Fig. 3(*p*) [20]		•		•				2.55	—	0.0027	—	—	0.403	—	—
Fig. 3(*q*) [54]		•		•				—	—	—	—	—	—	—	—
Fig. 3(*r*) [55,56]	•				•			0.65	—	0.056	82.6	82.6	—	2.48	2.48
Fig. 3(*s*) [57]	•				•			—	—	—	—	—	—	—	—
Fig. 3(*t*) [58]	•					•		—	—	—	—	—	—	—	—
Fig. 3(*u*) [58]	•					•		—	—	—	—	—	—	—	—
Fig. 3(*v*) [20]		•				•		—	—	—	—	—	—	—	—
Fig. 3(*w*) [59]	•					•		—	—	—	—	—	—	—	—
Fig. 3(*x*) [60–62]		•					•	—	—	—	—	—	—	—	—
Fig. 3(*y*) [63]		•					•	—	—	—	—	—	—	—	—
Fig. 3(*z*) [64]		•					•	—	—	—	—	—	—	—	—

Table 3 Geometric parameters values for compliant revolute joints

Compliant revolute joint	b (mm)	L, l_f (mm)	t, r (mm)	C, R, g, h_f (mm)	φ, φ_1, φ_2 (deg)
Figs. 3(*a*)–3(*d*)	10	9	1	4.5	—
Fig. 3(*e*)	10	9	1	2.25	—
Figs. 3(*f*)–3(*h*)	4	20	0.15	—	45
Figs. 3(*i*) and 3(*j*)	4	10	0.15	1	45
Fig. 3(*k*)	4	10	0.15	1	40, 50
Fig. 3(*l*)	8	10	0.15	—	—
Fig. 3(*m*)	4	10	0.15	0.2	—
Figs. 3(*o*) and 3(*p*)	4	10	0.15	2	—
Fig. 3(*r*)	—	10	0.15	3	—

even. However, the number of cylindrical joints in this joint is five which appears to be selected only to satisfy Kutzbach Grubler's degree of freedom formula to achieve a 1DOF mechanism. However, sometimes this formula leads to a wrong result which is quite different from the reality especially for spatial configurations like Double-Hooke's universal joint which is well-known as an overconstrained linkage.

4.2 Compliant Revolute Joints. The range of motion, the off-axis rotational stiffness to the on-axis rotational stiffness ratios, the axis drift, and the size of the compliant revolute joints compared. The values are normalized to the largest in the group, as shown in Fig. 7. Considering the range of motion, the largest values have been reached in multileaf, cross axis, and CR-3. As a general rule, the leaf spring and tap spring flexure joints have a large range of motion, compared to the notch type flexure joints. As can be seen in Fig. 7, the dimensionless ratios of off-axis rotational stiffness about Y-axis and X-axis to the on-axis rotational stiffness of compliant revolute joints ($\varepsilon_1 = K_{\theta y}/K_{\theta z}$ and $\varepsilon_2 = K_{\theta x}/K_{\theta z}$) are compared. It is noteworthy that both largest ratios were achieved in CR-1. Besides, both ratios are equal for CR-1, CR-2, and Split-Tube-1, due to the symmetrical design in XZ-plane and YZ-plane. For the notch type flexure joints, these ratios are smaller than leaf spring and tap spring flexure joints. Considering the axis drift, the cross axis has a very large axis drift and right-circular corner-filleted (RCCF) has very small axis drift. Furthermore, this feature is zero for some complex flexure joints with parallel combination like CR-1 and CR-2. Therefore, a symmetric design can be a solution to decrease the deviation of the rotational axis in complex flexures with parallel combination of flexible segments. An approach to increase the range of motion of compliant joints is using series combination of them. Generally, this method can increase the axis drift and decrease the dimensionless ratios of off-axis rotational stiffness to on-axis rotational stiffness which is not desired for a compliant revolute joint. These

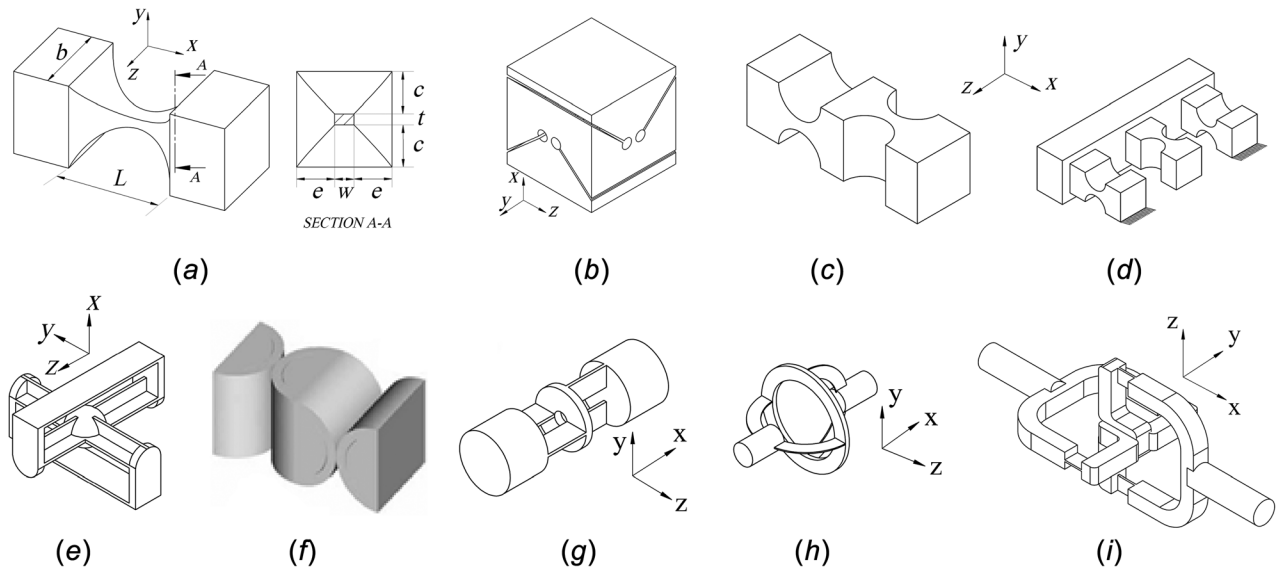

Fig. 4 Compliant universal joints; (*a*) two-axis flexure joint, (*b*) notch U joint-1, (*c*) notch U joint-2, (*d*) collinear notch joint, (*e*) CU joint, (*f*) XU-joint, (*g*) Stark-1, (*h*) Stark-2, and (*i*) compliant cardan U joint

Table 4 Overview of the compliant universal joints, with flexure type (indicated with •), range of motion, axis drift, on-axis and off-axis stiffness. Dash (—) denotes analytical data are not available; Intersecting axes and skew axes identified with ✓ and ✗, respectively. The configuration of each joint is shown in Fig. 4.

							Range of motion (rad)		Axis drift (μm)		On-axis stiffness (N·mm/rad $\times 10^{-3}$)		Off-axis stiffness	
Compliant universal joints	Primitive flexure	Complex flexure	Notch-type	Leaf-spring	Contact-base	Axes status	θ_z	θ_y	δ_z	δ_y	$K_{\theta z}$	$K_{\theta y}$	$K_{\theta x}$ (N·mm/rad $\times 10^{-3}$)	K_x (N/mm $\times 10^{-3}$)
Fig. 4(*a*) [66]	•		•			✓	—	—	—	—	—	—	—	—
Fig. 4(*b*)		•	•			✓	0.03	0.03	34	34	22.92	22.92	242.66	76.055
Fig. 4(*c*) [37,38]		•	•			✗	0.03	0.03	34	34	22.92	22.92	242.66	76.055
Fig. 4(*d*) [37,38]		•	•			✓	0.03	0.03	34	34	45.026	23.13	323.56	101.41
Fig. 4(*e*) [21]		•		•		✓	0.56	0.56	0	0	0.0585	0.0585	43.79	1.315
Fig. 4(*f*) [62]		•			•	✗	—	—	—	—	—	—	—	—
Fig. 4(*g*) [67]		•	•			✗	0.113	0.113	198.7	198.7	12.834	12.834	246.1	77.78
Fig. 4(*h*) [67]		•		•		✗	—	—	—	—	—	—	—	—
Fig. 4(*i*) [68]		•	•			✓	0.113	0.113	198.7	198.7	12.834	12.834	246.1	77.78

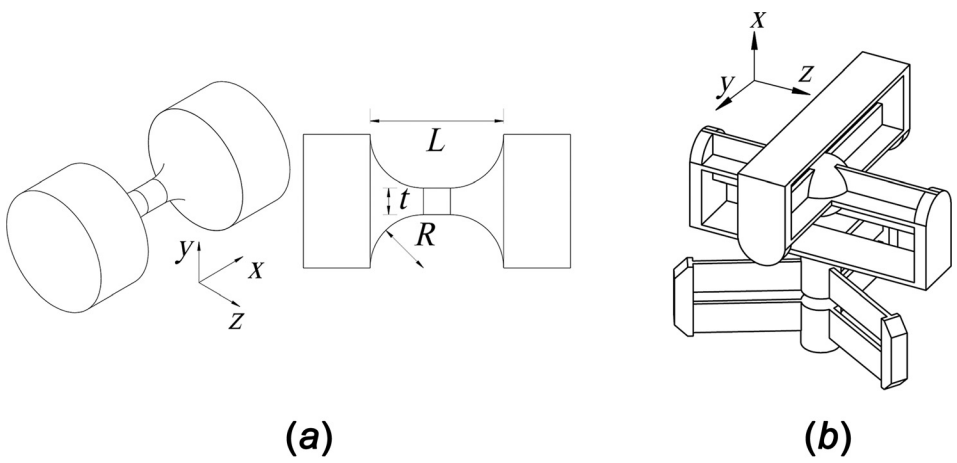

Fig. 5 Compliant spherical joints: (*a*) three-axis flexure joint and (*b*) CS joint

Table 5 Overview of the compliant spherical joints, with flexure type (indicated with •), range of motion, axis drift, and axial and off-axis stiffness. Dash (—) denotes analytical data are not available; the embodiment of each joint is shown in Fig. 5.

					Range of motion (rad)			Axis drift (μm)			Axial stiffness (N·mm/rad × 10^{-3})			Off-axis stiffness (N/mm × 10^{-3})
Compliant spherical joints	Primitive flexure	Complex flexure	Notch–type	Leaf-spring	θ_x	θ_y	θ_z	δ_x	δ_y	δ_z	$K_{\theta x}$	$K_{\theta y}$	$K_{\theta z}$	K_x
Fig. 5(*a*) [69]	•		•		0.166	0.0125	0.0125	—	—	—	27.58	19.8	19.8	49.5
Fig. 5(*b*) [21]		•		•	0.894	0.559	0.559	—	0	0	0.0083	0.0585	0.0585	9.059

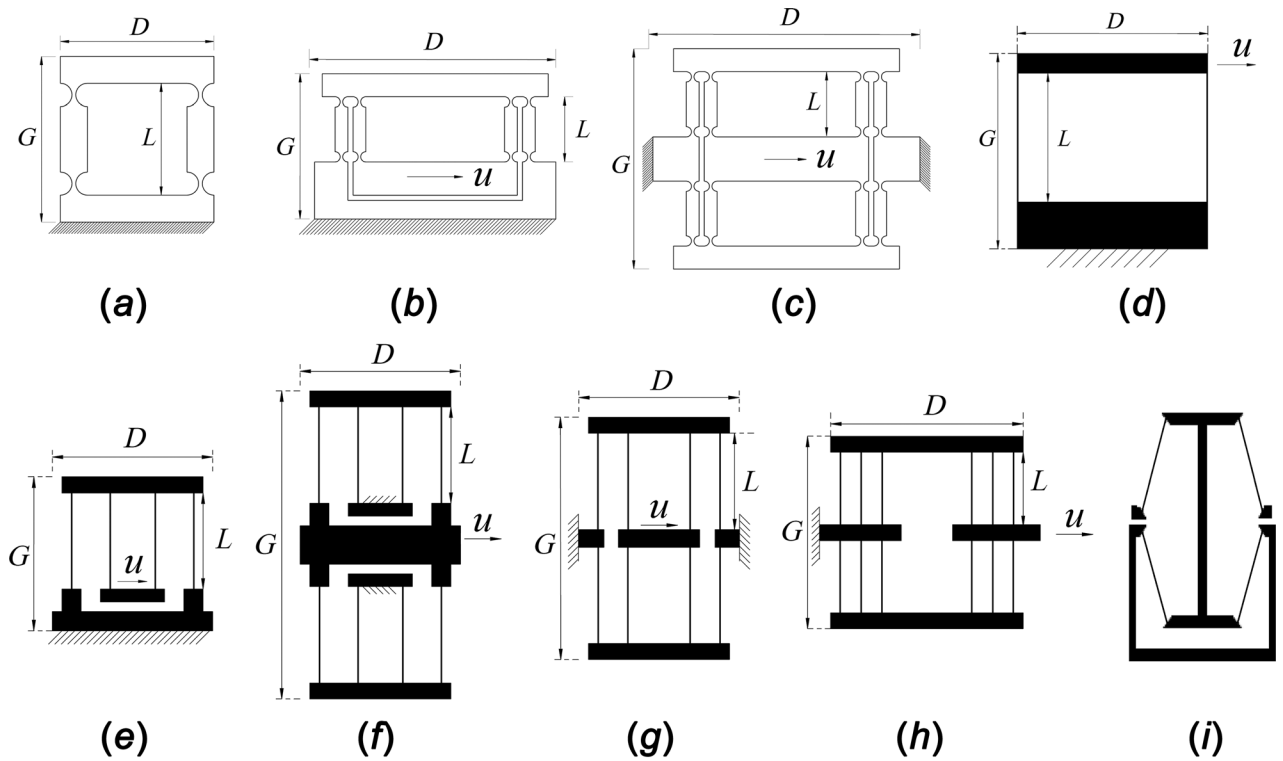

Fig. 6 Compliant translational joints: (*a*) four-bar-notch block and (*b*) double notch block, (*c*) symmetrical double notch block, (*d*) four-bar block, (*e*) double block, (*f*) symmetrical double block, (*g*) folded beam, (*h*) planar CT joint, and (*i*) double XBob

Table 6 Overview of the compliant translational joints, with flexure type (indicated with •), range of motion, dimensionless parameter, on-axis and off-axis stiffness. Dash (—) denotes analytical data are not available; the embodiment of each joint is shown in Fig. 6.

			Geometric parameters			Range of motion	Axial stiffness	Off-axis stiffness	Dimensionless parameter
			G	D	L	δ_x	K_x	K_y	
Compliant translational joints	Notch-type	Leaf-spring	(mm)			(mm)	N/mm × 10^{-3}		δ^*
Fig. 6(*a*) [37]	•		50	50	30	0.6	0.23	152.11	0.0085
Fig. 6(*b*) [37]	•		50	70	30	1.2	0.12	76.06	0.014
Fig. 6(*c*) [37]	•		70	70	30	1.2	0.23	152.11	0.012
Fig. 6(*d*) [73]		•	39	30	30	1.886	0.052	46.67	0.0383
Fig. 6(*e*) [74]		•	39	30	30	3.77	0.026	23.33	0.0766
Fig. 6(*f*) [74]		•	69	50	30	3.77	0.052	46.67	0.0443
Fig. 6(*g*) [70,72]		•	69	50	30	3.77	0.052	46.67	0.0443
Fig. 6(*h*) [21]		•	69	50	30	3.77	0.078	70	0.0443
Fig. 6(*i*) [72,75]		•	—	—	—	—	—	—	—

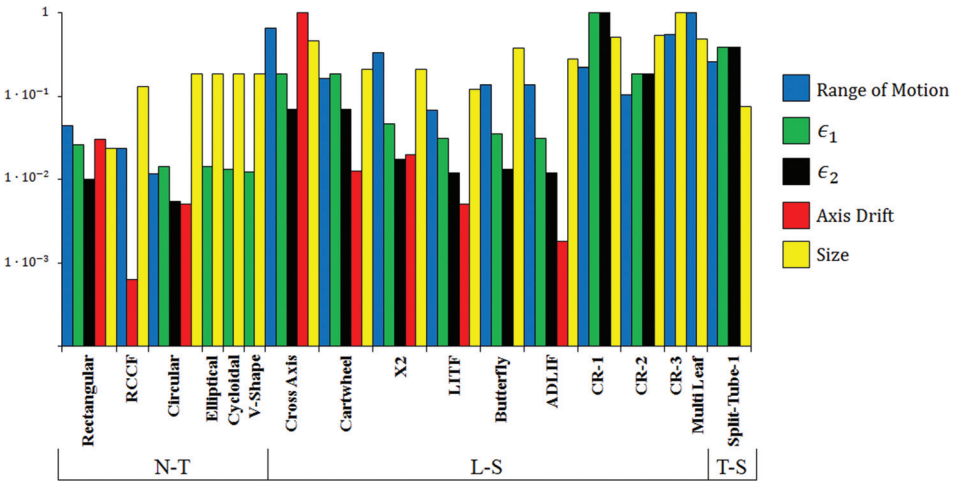

Fig. 7 The range of motion, the dimensionless ratios of off-axis rotational stiffness to on-axis rotational stiffness, axis drift, and size of each compliant revolute joint, if data were available. The values were normalized to the largest in the group, shown in logarithmic scale. The flexure types are notch-type (N-T), leaf-spring (L-S), and tap-spring (T-S).

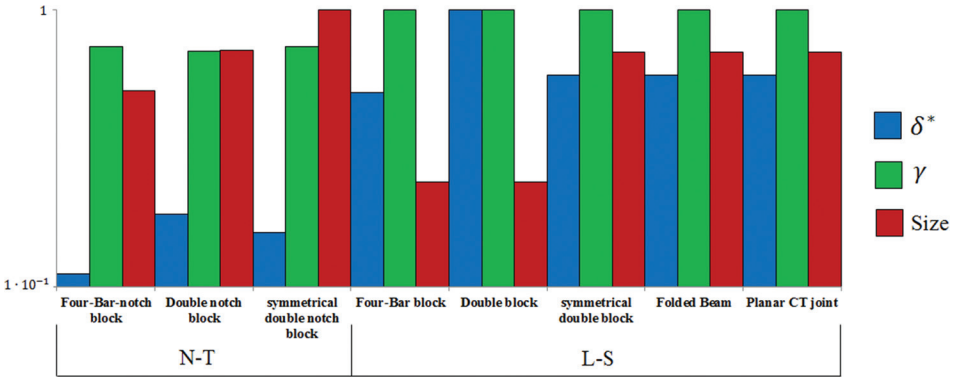

Fig. 8 The dimensionless ratio for range of motion (δ^*), the dimensionless ratio of off-axis translational stiffness to on-axis translational stiffness (γ), and size of each compliant translational joint, if data were available. The values were normalized to the largest in the group, shown in logarithmic scale. The flexure types are notch-type (N-T) and leaf-spring (L-S).

can be seen in X^2 joint which includes two Cartwheel joints in series. However, considering the results of ADLIF, which is a series combination of LITF, it can be seen the range of motion is increased, but the axis drift is decreased and the dimensionless ratios of off-axis rotational stiffness to on-axis rotational stiffness remain constant. ADLIF is designed as two LITF building blocks which are arranged antisymmetrically. Therefore, an antisymmetrical and inverted design can decrease the deviation of rotational axis in complex flexures with series combination of flexible segments.

4.3 Compliant Universal Joints. According to Table 4, the dimensionless ratios of off-axis rotational stiffness to the on-axis rotational stiffness ($\zeta_1 = K_{\theta x}/K_{\theta y}$ and $\zeta_2 = K_{\theta x}/K_{\theta z}$) are very large for the CU joint and $\zeta_1 = \zeta_2 = 749.05$. Besides, these ratios are smaller than 19 for other compliant universal joints. In the CU joint a large range of motion with zero axis drift are found, compared to the other cases. As can be seen in Table 4, for Notch U joint-2, X_U-Joint and Stark-1 and 2, rotation axes (Y-axis and Z-axis) are skew and these axes intersect each other in the other designs. As a general rule, by adding two compliant revolute joints together while their rotation axes are perpendicular, a compliant non-CV joint based on Hooke's universal joint will be produced.

4.4 Compliant Spherical Joints. First, the ratios of off-axis translational stiffness to the on-axis rotational stiffness ($\eta_1 = K_x/K_{\theta x}$, $\eta_2 = K_x/K_{\theta y}$, and $\eta_3 = K_x/K_{\theta z}$ in $(1/\text{mm}^2)$) for compliant spherical joints are compared. In the CS joint relatively large ratios are found, compared to the three-axis flexure joint, as can be seen in Table 5. The CS joint has a large range of motion with zero axis drift. As a general rule, a compliant spherical joint can be built by connecting three compliant revolute joints or one compliant universal joint with a compliant revolute joint. However, this kind of design uses a large space.

4.5 Compliant Translational Joints. The dimensionless ratios for range of motion (δ^*) and off-axis translational stiffness to on-axis translational stiffness ($\gamma = K_y/K_x$) and the size of the compliant translational joints are compared. The values are normalized to the largest in the group, as shown in Fig. 8. In translational joints with a symmetrical structure, the axis drift is improved and a relatively small δ^* and large size are found, compared to their primitive design. The dimensionless ratios δ^* and γ

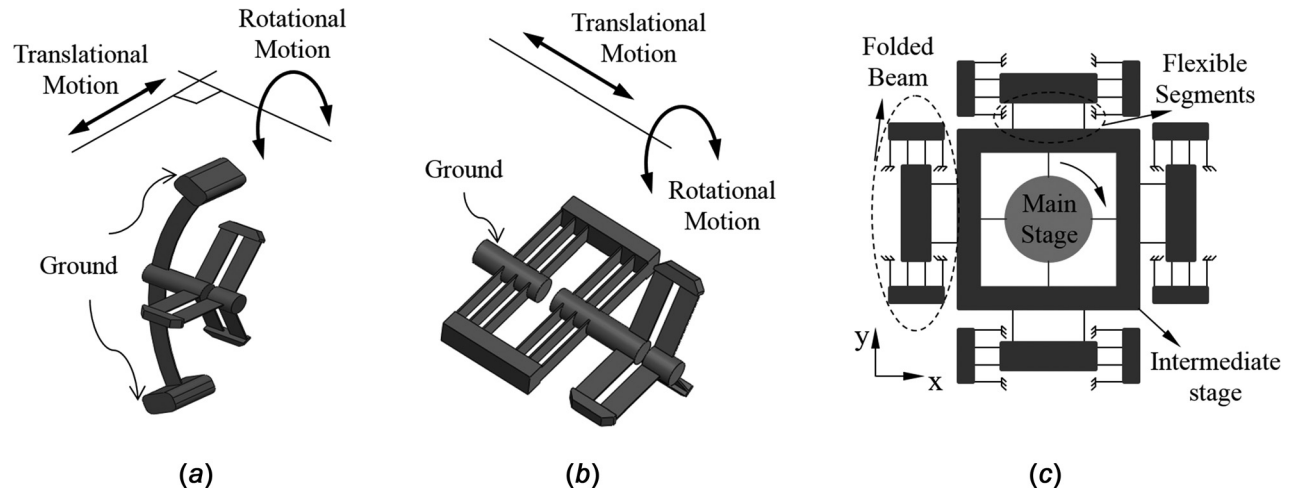

Fig. 9 Proposed: (*a*) compliant spherical fork joint, (*b*) compliant cylindrical joint, and (*c*) compliant planar joint as an example

for leaf spring are larger than in the notch type. If the structure of joints is being built as a sector of sphere, then a compliant spherical translational joint can be achieved.

4.6 Compliant Spherical Fork Joint, Compliant Cylindrical Joint, and Compliant Planar Joint. There are no equivalent compliant joints from the literature for spherical fork, cylindrical, and planar joints. However, we may achieve them by combining available compliant joints. For instance, as can be seen in Fig. 9(*a*), a compliant spherical fork joint can be built by connecting a compliant spherical translational joint with a compliant revolute joint in which their axes are perpendicular. Besides, a cylindrical compliant joint can be built by connecting a compliant translational joint and a compliant revolute joint if their axes are coincident and aligned as shown in Fig. 9(*b*). A compliant planar joint may be achieved, by arranging two compliant translational joints orthogonal and a compliant revolute joint. As shown in Fig. 9(*c*), the main stage has a rotation motion about *z*-axis respect to the intermediate stage which has two translational motions along the *x*-axis and *y*-axis. Therefore, the main stage has 3DOF and a compliant planar joint is achieved.

4.7 Compliant Homokinetic Couplings. Our results show, compliant universal joints are designed based on rigid-body Hooke's universal joint by rigid-body-replacement method.

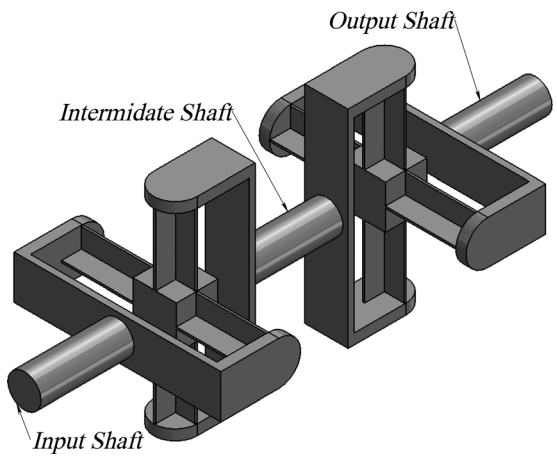

Fig. 10 Proposed compliant homokinetic coupling based on Double-Hooke's universal joint as an example

Therefore, if compliant form of the used rigid-body joints and combinations in a rigid-body CV joint exist or they can be reached by combining available compliant joints, then compliant homokinetic couplings can be designed based on the rigid-body CV joints by means of rigid-body-replacement method. For example, a Double-Hooke's universal joint is designed by arranging two rigid-body Hooke's universal joints. Therefore, by adding two arbitrary compliant universal joints from Fig. 4, several compliant homokinetic couplings based on rigid-body Double-Hooke's universal joint can be built, as shown in Fig. 10. Moreover, this method can be extended for converting other rigid-body CV joints such as Wier, Clemens, Altmann, etc., to a compliant structure which their rigid-body joints have an equivalent compliant joint. In another way, by means of the FACT method, many more designs for compliant homokinetic coupling can be obtained. The geometric requirement to design a compliant homokinetic coupling based on FACT method is symmetrical configuration of a compliant structure with two rotational DOF.

5 Conclusion

A review on rigid-body CV joints and different kinds of compliant joints, classification and comparison, were made toward the design of compliant homokinetic coupling. For the first time, the graph representation of rigid-body CV joints was studied and different types of used rigid-body joints and important combinations were found.

Moreover, several different kinds of compliant joints suitable to design a compliant homokinetic coupling were studied, classified, and compared for their stiffness, axis drift, and range of motion. In order to make a fair comparison, the joints were modeled analytically and same size and same material properties were used. Our results show all of the leaf spring compliant joints have large range of motion, large ratios of off-axis stiffness to on-axis stiffness and large size, in comparison to the notch type compliant joints. Moreover, the results show a symmetric design is efficient to decrease the axis drift in complex flexures with parallel combination of flexible segments and an antisymmetrical and inverted design can solve the deviation of rotational axis in complex flexures with series combination of flexible segments.

It was shown that in the literature there are no equivalent compliant joints for some rigid-body joints and combinations such as cylindrical, planar, spherical fork, and spherical parallelogram quadrilateral joints. However, we have demonstrated they can be obtained by combining available compliant rotational and translational joints. Moreover, it was shown that many more compliant

homokinetic couplings can be achieved by means of rigid-body-replacement method and FACT method.

References

[1] Moon, Y. M., and Kota, S., 2002, "Design of Compliant Parallel Kinematic Machines," ASME Paper No. DETC2002/MECH-34204.

[2] Perry, J. C., Oblak, J., Jung, J. H., Cikajlo, I., Veneman, J. F., Goljar, N., Bizovicar, N., Matjacic, Z., and Keller, T., 2011, "Variable Structure Pantograph Mechanism With Spring Suspension System for Comprehensive Upper-Limb Haptic Movement Training," J. Rehab. Res. Dev., **48**(4), pp. 317–334.

[3] Ishii, C., and Kamei, Y., 2008, "On Servo Experiment of a New Multi-DOF Robotic Forceps Manipulator for Minimally Invasive Surgery," Proceeding of the 5th International Symposium on Mechanics and Its Applications, Amman, Jordan, May 27–29, pp. 1–6.

[4] Chiang, C. H., 1988, *Kinematics of Spherical Mechanisms*, Cambridge University Press, Cambridge, UK.

[5] Hunt, K. H., 1973, "Constant-Velocity Shaft Couplings: A General Theory," J. Eng. Ind., **95**(B), pp. 455–464.

[6] Rzeppa, A. H., 1928, "Constant Velocity Universal Joint," U.S. Patent No. 1,665,280.

[7] Culver, I. H., 1969, "Constant Velocity Universal Joint," U.S. Patent No. 3,477,249.

[8] Thompson, G. A., 2006, "Constant Velocity Coupling and Control System Therefore," U.S. Patent No. 7,144,326.

[9] Kocabas, H., 2007, "Design and Analysis of a Spherical Constant Velocity Coupling Mechanism," ASME J. Mech. Des., **129**(9), pp. 991–998.

[10] Howell, L. L., 2001, *Compliant Mechanisms*, Wiley, New York, p. 459.

[11] Herder, J. L., and Van Den Berg, F. P. A., 2000, "Statically Balanced Compliant Mechanisms (SBCM's), and Example and Prospects," Proceedings ASME DETC 26th Biennial, Mechanisms and Robotics Conference, Baltimore, MD, ASME Paper No. DETC2000/MECH-14144, pp. 553–560.

[12] Berglund, M. D., Magleby, S. P., and Howell, L. L., 2000, "Design Rules for Selecting and Designing Compliant Mechanisms for Rigid-Body Replacement Synthesis," Proceedings of the 26th Design Automation Conference, ASME DETC, Baltimore, MD, 14225.

[13] Howell, L. L., and Midha, A., 1994, "A Method for the Design of Compliant Mechanisms With Small-Length Flexural Pivots," ASME J. Mech. Des., **116**(1), pp. 280–290.

[14] Hopkins, J. B., 2007, "Design of Parallel Flexure Systems via Freedom and Constraint Topologies (FACT)," Master thesis, Massachusetts Institute of Technology, Cambridge, MA.

[15] Hopkins, J. B., and Culpepper, M. L., 2010, "Synthesis of Multi-Degree of Freedom Flexure System Concepts via Freedom and Constraint Topologies (FACT)—Part I: Principles," J. Precis. Eng., **34**(2), pp. 259–270.

[16] Martin, G. H., 1982, *Kinematics and Dynamics of Machines*, McGraw-Hill Book Company, New York.

[17] Molly, H., and Bengisu, O., 1969, "Das Gleichgang–Gelenk im Symmetriespiegel (The Constant Velocity Joint in the Mirror of Symmetry)," Automob. Ind., **14**(2), pp. 45–54.

[18] McCarthy, J. M., and Soh, G. S., 2010, *Geometric Design of Linkages*, 2nd ed., Springer, New York.

[19] Xu, P., Jingjun, Y., Guanghua, Z., and Shusheng, B., 2007, "The Modeling of Leaf-Type Isosceles-Trapezoidal Flexural Pivots," ASME Paper No. DETC2007-34981.

[20] Jingjun, Y., Xu, P., Minglei, S., Shanshan, Z., Shushing, B., and Guanghua, Z., 2009, "A New Large–Stroke Compliant Joint & Micro/Nano Positioner Design Based on Compliant Building Blocks," ASME/IFToMM International Conference on Reconfigurable Mechanisms and Robots, London, UK, June 22–24, pp. 409–416.

[21] Trease, B. P., Moon, Y. M., and Kota, S., 2005, "Design of Large-Displacement Compliant Joints," ASME J. Mech. Des., **127**(4), pp. 788–798.

[22] Hunt, K. H., 1983, "Structural Kinematics of In-Parallel-Actuated Robot-Arms," ASME J. Mech. Des., **105**(4), pp. 705–712.

[23] Rineer, A. E., 1979, "Constant Velocity Universal Joint," U.S. Patent No. 4,133,189.

[24] Sclater, N., and Chironis, N. P., 2001, *Mechanisms and Mechanical Devices Sourcebook*, 3rd ed., McGraw-Hill Book Company, New York.

[25] Geisthoff, H., Welschof, H., and Herchenbach, P., 1966, "Quasi Homokinetic Double Hooke," German Patent No. 1,302,735.

[26] Geisthoff, H., Welschof, H., and Herchenbach, P., 1978, "Strictly Homokinetic Double Hooke," German Patent No. 2,802,572.

[27] Wier, F. L., 1968, "Constant Velocity Universal Joint," U.S. Patent No. 3,385,081.

[28] Fenaille, P., 1927, "Tracta Joint," German Patent No. 617,356.

[29] Fischer, I. S., 1999, "Numerical Analysis of Displacements in a Tracta Coupling," J. Eng. Comput., **15**(4), pp. 334–344.

[30] Freudenstein, F., and Maki, E. R., 1979, "Creation of Mechanisms According to Kinematic Structure and Function," Environ. Plann. B, **6**(4), pp. 375–391.

[31] Dodge, A. Y., 1941, "Constant Velocity Universal Joint," U.S. Patent No. 2,255,762.

[32] Baker, M. P., 1966, "Constant Velocity Universal Joint," U.S. Patent No. 3,263,447.

[33] Eccher, O. B., 1970, "Constant Velocity Universal Joint," U.S. Patent No. 3,517,528.

[34] Falk, J. B., 1975, "High Deflection Constant Speed Universal Joint," U.S. Patent No. 3,924,420.

[35] Yaghoubi, M., Mohtasebi, S. S., Jafary, A., and Khaleghi, H., 2011, "Design, Manufacture and Evaluation of a New and Simple Mechanism for Transmission of Power Between Intersecting Shafts up to 135 Degrees (Persian Joint)," J. Mech. Mach. Theory, **46**(7), pp.861–868.

[36] Lobontiu, N., 2002, *Compliant Mechanisms Design of Flexure Hinges*, CRC Press, New York, pp. 72–82.

[37] Paros, J. M., and Weisbord, L., 1965, "How to Design Flexure Hinges," Mach. Des., **37**, pp. 151–156.

[38] Smith, S. T., 2000, *Flexures: Elements of Elastic Mechanisms*, Gordon and Breach Science, New York.

[39] Dirksen, F., and Lammering, R., 2011, "On Mechanical Properties of Planar Flexure Hinges of Compliant Mechanisms," J. Mech. Sci., **2**, pp. 109–117.

[40] Chen, G. M., Jia, J. Y., and Li, Z. W., 2005, "Right-Circular Corner-Filleted Flexure Hinges," IEEE International Conference on Automation Science and Engineering, Edmonton, Canada, Aug. 1–2, pp. 249–253.

[41] Lobontiu, N., Paine, J. S. N., Malley, E. O., and Samuelson, M., 2002, "Parabolic and Hyperbolic Flexure Hinges: Flexibility, Motion Precision and Stress Characterization Based on Compliance Closed-Form Equations," J. Precis. Eng., **26**(2), pp. 183–192.

[42] Lobontiu, N., Paine, J. S. N., Garcia, E., and Goldfarb, M., 2002, "Design of Symmetric Conic-Section Flexure Hinges Based on Closed-Form Compliance Equations," J. Mech. Mach. Theory, **37**(5), pp. 477–498.

[43] Smith, S. T., Badami, V. G., Dale, J. S., and Xu, Y., 1997, "Elliptical Flexure Hinges," Rev. Sci. Instrum., **68**(3), pp. 1474–1483.

[44] Tian, Y., Shirinzadeh, B., Zhang, D., and Zhong, Y., 2010, "Three Flexure Hinges for Compliant Mechanism Designs Based on Dimensionless Graph Analysis," J. Precis. Eng., **34**(1), pp. 92–100.

[45] Haringx, J. A., 1949, "The Cross Spring Pivot as a Constructional Element," Appl. Sci. Res., **1**(1), pp. 313–332.

[46] Jensen, B. D., and Howell, L. L., 2002, "The Modeling of Cross-Axis Flexural Pivots," J. Mech. Mach. Theory, **37**(5), pp. 461–476.

[47] Martin, J., and Robert, M., 2011, "Novel Flexible Pivot With Large Angular Range and Small Center Shift to be Integrated Into a Bio-Inspired Robotic Hand," J. Intell. Mater. Syst. Struct., **22**(13), pp. 1431–1437.

[48] Xu, P., Jingjun, Y., Guanghua, Z., Shusheng, B., and Zhiwei, Y., 2008, "Analysis of Rotational Precision for an Isosceles-Trapezoidal Flexural Pivot," ASME J. Mech. Des., **130**(5), p. 052302.

[49] Xu, P., Jingjun, Y., Guanghua, Z., and Shusheng, B., 2008, "The Stiffness Model of Leaf-Type Isosceles Trapezoidal Flexural Pivots," ASME J. Mech. Des., **130**(8), p. 082303.

[50] Xu, P., Jingjun, Y., Guanghua, Z., and Shusheng, B., 2009, "A Novel Family of Leaf-Type Compliant Joints: Combination of Two Isosceles-Trapezoidal Flexural Pivots," ASME J. Mech. Rob., **1**(2), p. 021005.

[51] Xu, P., and Jingjun, Y., 2011, "ADLIF: A New Large-Displacement Beam-Based Flexure Joint," J. Mech. Sci., **2**, pp. 183–188.

[52] Henein, S., Droz, S., Myklebust, L., and Onillon, E., 2003, "Flexure Pivot for Aerospace Mechanisms," Proceedings of the 10th European Space Mechanisms and Tribology Symposium, Sept. 24–26, San Sebastian, Spain, pp. 1–4.

[53] Wiersma, D. H., Boer, S. E., Aarts, R. G. K. M., and Brouwer, D. M., 2012, "Large Stroke Performance Optimization of Spatial Flexure Hinges," ASME Paper No. DETC2012-70502.

[54] Fowler, R. M., 2012, "Investigation of Compliant Space Mechanisms With Application to the Design of a Large-Displacement Monolithic Compliant Rotational Hinge," Master thesis, Brigham Young University, Provo, UT.

[55] Goldfarb, M., and Speich, J. E., 1999, "A Well-Behaved Revolute Flexure Joint for Compliant Mechanism Design," ASME J. Mech. Des., **121**(3), pp. 424–429.

[56] Goldfarb, M., and Speich, J. E., 2003, "Split Tube Flexure," U.S. Patent No. 6,585,445.

[57] Qizhi, Y., Xiaobing, Z., Long, C., and Pengfei, Z., 2011, "Analysis of Traditional Revolute Pair and the Design of a New Compliant Joint," International Conference on Electric Information and Control Engineering (ICEICE), Wuhan, China, Apr. 15–17, pp. 2007–2009.

[58] Berselli, G., Piccinini, M., and Vassura, G., 2011, "Comparative Evaluation of the Selective Compliance in Elastic Joints for Robotic Structures," IEEE International Conference on Robotics and Automation, Shanghai, China, May 9–13, pp. 4626–4631.

[59] Balucani, M., Belfiore, N. P., Crescenzi, R., and Verotti, M., 2010, "The Development of a MEMS/NEMS-based 3 D.O.F. Compliant Micro Robot," Proceedings of the 19th International Workshop on Robotics in Alpe-Adria-Danube Region, Budapest, Hungary, June 24–26 pp. 173–179.

[60] Hillberry, B. M., and Hall, A. S., 1976, "Rolling Contact Prosthetic Knee Joint," U.S. Patent No. 3,945,053.

[61] Mankame, N. D., and Ananthasuresh, G. K., 2002, "Contact Aided Compliant Mechanisms: Concept and Preliminaries," ASME Paper No. DETC2002/MECH-34211.

[62] Jeanneau, A., Herder, J. L., Laliberte, T., and Gosselin, C., 2004, "A Compliant Rolling Contact Joint and Its Application in a 3-DOF Planar Parallel Mechanism With Kinematic Analysis," ASME Paper No. DETC2004-57264.

[63] Cannon, J. R., and Howell, L. L., 2005, "A Compliant Contact-Aided Revolute Joint," J. Mech. Mach. Theory, **40**(11), pp. 1273–1293.

[64] Cannon, J. R., Lusk, C. P., and Howell, L. L., 2005, "Compliant Rolling-Contact Element Mechanisms," ASME Paper No. DETC2005-84073.

[65] See supplementary material Appendices A, B, C, and D for the related formulas for the given results in Table 2, Table 4, Table 5, and Table 6, respectively.
[66] Lobontiu, N., and Garcia, E., 2003, "Two-Axis Flexure Hinges With Axially-Collocated and Symmetric Notches," Comput. Struct., **81**(13), pp. 1329–1341.
[67] Stark, J. A., 1958, "Flexible Couplings," U.S. Patent No. 2,860,495.
[68] Tanik, E., and Parlaktas, V., 2012, "Compliant Cardan Universal Joint," ASME J. Mech. Des., **134**(2), p. 021011.
[69] Lobontiu, N., and Paine, J. S. N., 2002, "Design of Circular Cross-Section Corner-Filleted Flexure Hinges for Three-Dimensional Compliant Mechanisms," ASME J. Mech. Des., **124**(3), pp. 479–484.
[70] Cannon, B. R., Lillian, T. D., Magleby, S. P., Howell, L. L., and Linford, M. R., 2005, "A Compliant End-Effector for Microscribing," Precis. Eng., **29**(1), pp. 86–94.
[71] Lin, Y. T., and Lee, J. J., 2007, "Structural Synthesis of Compliant Translational Mechanisms," 12th IFToMM World Congress, Besancon, France, June 18–21, pp. 1–5.
[72] Mackay, A., 2007, "Large Displacement Linear Motion Compliant Mechanisms," Master's thesis, Brigham Young University, Provo, UT.
[73] Jones, R. V., 1951, "Parallel and Rectilinear Spring Movements," J. Sci. Instrum., **28**(2), pp. 38–41.
[74] Kyusojin, A., and Sagawa, D., 1988, "Development of Linear and Rotary Movement Mechanism by Using Flexible Strips," Bull. Jpn. Soc. Precis. Eng., **22**(4), pp. 309–314.
[75] Hubbard, N. B., Wittwer, J. W., Kennedy, J. A., Wilcox, D. L., and Howell, L. L., 2004, "A Novel Fully Compliant Planar Linear-Motion Mechanism," ASME Paper No. DETC2004-57008.